

Detection of visible light from the darkest world

David M. Kipping¹ & David S. Spiegel²

¹*Center for Astrophysics, 60, Garden Street, Cambridge, MA 02138 [E-mail: dkippling@cfa.harvard.edu]*

²*Department of Astrophysical Sciences, Peyton Hall, Princeton University, Princeton, NJ 08544*

Accepted 2011 August 1. Received 2011 July 25; in original form 2011 June 29

ABSTRACT

We present the detection of visible light from the planet TrES-2b, the darkest exoplanet currently known. By analysis of the orbital photometry from publicly available *Kepler* data (0.4–0.9 μm), we determine a day-night contrast amplitude of 6.5 ± 1.9 ppm, constituting the lowest amplitude orbital phase variation discovered. The signal is detected to 3.7σ confidence and persists in six different methods of modelling the data and thus appears robust. In contrast, we are unable to detect ellipsoidal variations or beaming effects, but we do provide confidence intervals for these terms. If the day-night contrast is interpreted as being due to scattering, it corresponds to a geometric albedo of $A_g = 0.0253 \pm 0.0072$. However, our models indicate that there is a significant emission component to day-side brightness, and the true albedo is even lower ($< 1\%$). By combining our measurement with *Spitzer* and ground-based data, we show that a model with moderate redistribution ($P_n \simeq 0.3$) and moderate extra optical opacity ($\kappa' \simeq 0.3 - 0.4$) provide a compatible explanation to the data.

Key words: techniques: photometric — stars: individual (TrES-2)

1 INTRODUCTION

Orbital photometric phase variations have long been used in the study and characterisation of eclipsing binaries (Wilson 1994), where the large masses and small orbital radii result in phase variations at the magnitude to millimagnitude level. The three dominant components of these variations are i) ellipsoidal variations, due to the non-spherical nature of a star caused by gravitational distortion (e.g. Welsh et al. 2010) ii) relativistic beaming, due to the radial motion of the star shifting the stellar spectrum (e.g. Maxted et al. 2000) iii) reflected/emitted light, which varies depending on what phase of a body is visible (e.g. For et al. 2010).

The visible bandpass orbital phase variations of a star due to a hot-Jupiter companion are much smaller - around the part-per-million (ppm) level - and thus have eluded detection until relatively recently. The high precision space-based photometry of CoRoT (0.56–0.71 μm) (Baglin et al. 2009) and *Kepler* (Basri et al. 2005) have opened up this exciting new way of studying exoplanets for first time, with several detections recently reported in the literature:

- CoRoT-1b (Snellen et al. 2009); reflected/emitted light amplitude 126 ± 36 ppm
- HAT-P-7b (Welsh et al. 2010); ellipsoidal amplitude 37 ppm, reflected/emitted light amplitude 63.7 ppm
- CoRoT-3b (Mazeh & Faigler 2010); ellipsoidal amplitude (59 ± 9) ppm, beaming amplitude (27 ± 9) ppm
- Kepler-7b (Demory et al. 2011); reflected/emitted light amplitude (42 ± 4) ppm

In this letter, we investigate the hot-Jupiter orbiting the G0V star TrES-2 (O’Donovan et al. 2006), where we detect a reflected/emitted light amplitude of (6.5 ± 1.9) ppm to a confidence of 3.7σ , or 99.98%. We also measure the ellipsoidal variation and relativistic beaming amplitudes to be (1.5 ± 0.9) ppm and (0.2 ± 0.9) ppm respectively, which are broadly consistent with theoretical expectation.

If our detected signal is interpreted as being purely due to scattering, then the corresponding geometric albedo would be $A_g = 0.0253 \pm 0.0072$ (using system parameters from Table 2, column 2 of Kipping & Bakos 2011 (KB11), as will be done throughout this work), meaning that just four months of *Kepler*’s exquisite photometry has detected light from the darkest exoplanet yet found. Extrapolating to a 6 year baseline, one can expect to detect albedos ≥ 0.1 (to 3σ confidence) at similar orbital radii down to $R_P \simeq 3.0 R_\oplus$. This clearly highlights the extraordinary potential which would be granted by an extended mission for *Kepler*.

2 OBSERVATIONS & ANALYSIS

2.1 Data Acquisition

We make use of “Data Release 3” (DR3) from the *Kepler Mission*, which consists of quarters 0, 1 and 2 (Q0, Q1 & Q2). Full details on the data processing pipeline can be found in the DR3 handbook. The data includes the use of BJD (Barycentric Julian Date) time stamps for each flux measurement, which is crucial for time sensitive measurements. All data used are publicly available via MAST.

We use the “raw” (labelled as “AP_RAW_FLUX” in the header) short-cadence (SC) data processed by the DR3 pipeline and a detailed description can be found in the accompanying release notes. The “raw” data has been subject to PA (Photometric Analysis), which includes cleaning of cosmic ray hits, Argabrightenings, removal of background flux, aperture photometry and computation of centroid positions. It does not include PDC (Pre-search Data Conditioning) algorithm developed by the DAWG (Data Analysis Working Group). As detailed in DR3, this data is not recommended for scientific use, owing to, in part, the potential for under/over-fitting of the systematic effects.

2.2 Cleaning of the Data

The raw data exhibit numerous systematic artifacts, including pointing tweaks (jumps in the photometry), safe mode recoveries (exponential decays) and focus drifts (long-term trends). The first effect may be corrected by applying an offset surrounding the jump, computed using a 30-point interpolative function either side. Due to the exponential nature of the second effect, we chose to exclude the affected data rather than attempt to correct it. The third effect may be corrected for using a detrending technique.

For this latter effect, we use the cosine filter utilised to detect ellipsoidal variations in CoRoT data by Mazeh & Faigler (2010). The technique acts as a high-pass filter allowing any frequencies of the orbital period or higher through and all other long-term trends are removed. Thus, we protect any physical flux variations on the time scale of interest. We applied the filter independently to Q0+Q1 data and then Q2 data. This is because the *Kepler* spacecraft was rotated in the intervening time and so the long-term trend will not be continuous over this boundary. After removing 3σ outliers with a running 20-point median and transits using the ephemeris of KB11, we applied the filter, with the resulting fitted trends shown in Fig 1. Our final cleaned data consists of 154,832 SC measurements with a mean SNR $\simeq 4408$.

2.3 Three Models

We first define our null hypothesis, \mathcal{M}_1 , where we employ a flat line model across the entire time series, described by a constant a_0 . For a physical description of the orbital phase variations, we first tried the same model as that used by Sirko & Paczynski (2003) and Mazeh & Faigler (2010). This simple model is sufficient for cases where one is dealing with low signal-to-noise and reproduces the broad physical features. The model, \mathcal{M}_2 , is given by

$$\mathcal{M}_2(\phi) = a_0 + 0.5a_{1c} \cos(\phi) + a_{1s} \sin(\phi) + a_{2c} \cos(2\phi) + a_{2s} \sin(2\phi), \quad (1)$$

where ϕ is the orbital phase (defined as being 0 at the time of transit minimum) and a_i are coefficients related to the physical model. a_0 is simply a constant to remove any DC (direct-current) component in the data. a_{1c} corresponds to the reflection/emission effect and is expected to have a negative amplitude. a_{1s} corresponds to the relativistic beaming effect and is expected to be positive. a_{2c} corresponds to the ellipsoidal variations and should be negative. a_{2s} is a

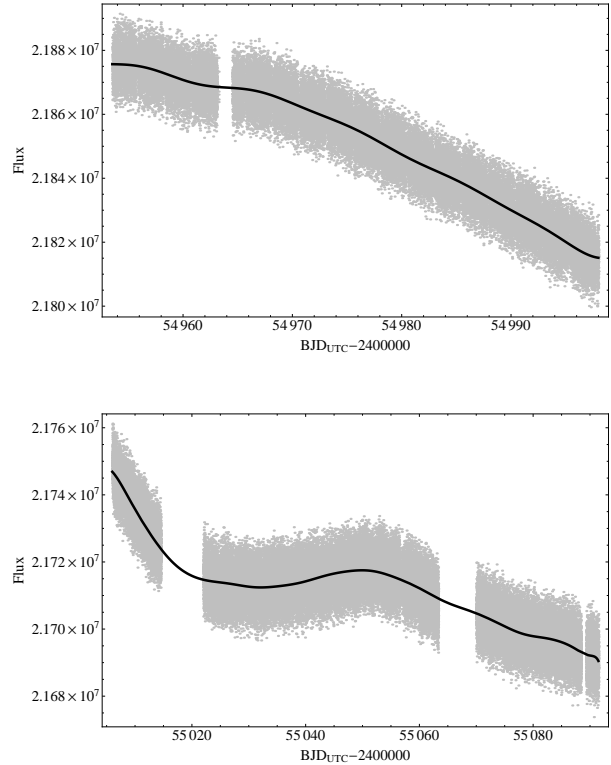


Figure 1. “Raw” (PA output) flux from DR3 of the Kepler pipeline for Q0&Q1 (upper panel) and Q2 (lower panel) of the star TrES-2. Overlaid is our model for the long-term trend, computed using a discrete cosine transform for each data set. Outliers and discontinuous systematic effects have been excluded.

dummy term which should be zero and ensures the ellipsoidal variation is detected with the correct phase.

We also tried a third model, \mathcal{M}_3 , where the a_{1c} term is replaced by the reflection caused by a Lambertian sphere:

$$0.5a_{1c} \cos \phi \rightarrow a_{1c} \left[\frac{\sin |\phi| + (\pi - |\phi|) \cos |\phi|}{\pi} \right]. \quad (2)$$

2.4 Three Data Modes

In addition to three models, we have three data input modes. The first is simply corrected for detrending and nothing else, denoted \mathcal{D}_1 . The second mode renormalises each orbital period epoch. This renormalisation is done by computing the median of each epoch and dividing each segmented time series by this value and we denote this mode as \mathcal{D}_2 . Finally, we tried allowing each orbital period epoch to have its own variable renormalisation parameter, which is simultaneously fitted to the data along with the orbital phase curve model. This parameter is dubbed $a_{0,j}$ for the j^{th} orbital period epoch. Denoting this data input mode as \mathcal{D}_3 , the fits now include an additional 51 free parameters.

The models are fitted to the unbinned data using a Markov Chain Monte Carlo algorithm described in KB11 (method A) with 1.25×10^5 accepted trials burning out the first 25,000. In total, there are nine ways of combining the

three models with the three data modes. All nine models are fitted and results are given in Table 1, with our preferred model description being \mathcal{M}_2 , \mathcal{D}_3 (since thermal emission is likely dominant over scattering, see §4).

3 RESULTS

3.1 Orbital Photometry

Table 1 presents the results of fitting the detrended *Kepler* photometry. Our models make no prior assumption on the sign or magnitude of the a_i coefficients. The orbital period and transit epoch are treated as Gaussian priors from the circular orbit results of KB11.

When considering statistical significance, what one is really interested in is the confidence of detecting each physical effect i.e. reflection/emission, ellipsoidal and beaming. For this reason, model comparison tools, such as the Bayesian Information Criterion (BIC) or an F-test are inappropriate. This is because these methods evaluate the preference of one hypothesis over another, where the two models would be a null-hypothesis and a hypothesis including reflection/emission, ellipsoidal variations, beaming and the dummy term. Thus, any inference drawn from this would be for the *entire* model and not for each individual effect. In the analysis presented here, simple inspection of the posteriors from Fig 2 shows that only one effect is actually detected (reflection/emission), but a model comparison method would evaluate the significance of all four physical effects (including the dummy term) versus no effect.

A more useful statistical test would consider the significance of each physical effect individually from a joint fit. An excellent tool to this end is the odds ratio test discussed in Kipping et al. (2010). If a parameter was equal to zero, we would expect 50% of the MCMC runs to give a positive value and 50% to give a negative value. Consider that some asymmetry exists and a fraction f of all MCMC trial were positive and $1 - f$ were negative. The reverse could also be true and so we define f such that $f > 0.5$ i.e. it represents the majority of the MCMC trials. The odds ratio of the asymmetric model over the 50:50 model is:

$$O = \frac{0.5}{1 - f} \quad (3)$$

For only two possible models, the probability of the asymmetric model being the correct one is $P(\text{asym}) = 1 - [1/(1 + O)]$. We perform this test on each of the four parameters fitted for, a_{1c} , a_{2c} , a_{1s} and a_{2s} . The associated results are visible in the top-left corners of each posterior shown in Fig 2, for our preferred model and data mode i.e. \mathcal{M}_2 , \mathcal{D}_3 . To summarise, only one parameter presents a significant detection - the reflection/emission effect. Here, we find a_{1c} 's posterior is sufficiently asymmetric to have a probability of occurring by random chance of just 0.02%, which equates to 3.67σ . We consider any signal detected above 3σ confidence to merit the claim of a "detection" rather than a measurement and thus we find TrES-2b to be the darkest exoplanet from which visible light has been detected.

As discussed in §2.3, we tried two different models for the reflection/emission effect; a simple sinusoid (\mathcal{M}_2) and the reflected light from a perfectly Lambertian sphere (\mathcal{M}_3). Between the two models, there is negligible difference in

the goodness-of-fit, as seen in Table 1, for all three data modes. Including the Lambertian model takes some power away from the ellipsoidal variations though and thus the current data does not yield a preference between a Lambertian sphere model or stronger ellipsoidal variations.

3.2 Occultation Measurement

The duration of the transit, and thus occultation since TrES-2b maintains negligible eccentricity, is equal to 4624 ± 42 seconds (defined as the time between when the planet's centre crosses the stellar limb to exiting under the same condition). In contrast, the orbital period of TrES-2b is 2.470619 days. We therefore obtain ~ 46 times more integration time of the orbit than the occultation event. This indicates that we should expect to be able to reach a sensitivity of $\sqrt{46}$ times greater, purely from photon statistics. The uncertainty on our phase curve measurement is ± 1.9 ppm. We therefore estimate that one should have an uncertainty on the occultation depth of ~ 13 ppm. If we assume the night-side has a negligible flux, then the depth of the occultation is expected to be 6.5 ppm (i.e. equal to the day-night contrast), and this already suggests that the present publicly available *Kepler* photometry will be insufficient to detect the occultation. To test this hypothesis, we will here fit the occultation event including the Q0, Q1 and Q2 data.

To perform our fit, we use the same Gaussian priors on P and τ as earlier. We also adopt priors for other important system parameters from KB11, such as $b = 0.8408 \pm 0.0050$, $p^2 = 1.643 \pm 0.067\%$ and $\tilde{T}_1 = 4624 \pm 42$ seconds. We stress that these are all priors and not simply fixed parameters. We also make use of the priors on the $a_{0,j}$ coefficients from the \mathcal{M}_3 , \mathcal{D}_3 fit. Data are trimmed to be within ± 0.06 days of the expected time of occultation to prevent the phase curve polluting our signal, leaving us with 8457 SC measurements. Assuming a circular orbit, the data were fitted using an MCMC algorithm.

The marginalised posterior of the occultation depth yields $\delta_{\text{occ}} = 16^{+13}_{-14}$ ppm, which is clearly not a significant detection. The derived uncertainty of 13-14 ppm is very close to our estimation of ~ 13 ppm and thus supports our hypothesis that the current *Kepler* data are insufficient to detect the occultation of TrES-2b. We also note that the inclusion of the Q2 data does improve the constraints on the occultation event (KB11 found $\delta_{\text{occ}} = 21^{+23}_{-22}$ ppm using Q0 & Q1 only).

4 DISCUSSION

Hot-Jupiters are generally expected to be dark. Significant absorption due to the broad wings of the sodium and potassium D lines is thought to dominate their visible spectra (Sudarsky et al. 2000), leading to low albedos of a few percent. Indeed, aside from the recent report of Kepler-7b's ($38 \pm 12\%$) *Kepler*-band geometric albedo (KB11), searches for visible light from hot-Jupiters have generally revealed mere upper limits (Collier Cameron et al. 2002; Leigh et al. 2003; Rowe et al. 2008; Burrows et al. 2008).

The 6.5 ± 1.9 ppm contrast (determined from our preferred model \mathcal{M}_2 , \mathcal{D}_3) between the day-side and night-side photon flux that we measure for TrES-2b represents the most sensitive measurement yet of emergent radiation in the visible from a hot-Jupiter, and is a factor of ~ 20 and ~ 6 dimmer than the corresponding differences for HAT-P-7b (Welsh et al. 2010) and Kepler-7b.

Table 1. Results of three models with three data modes, giving nine sets of results. Emboldened row denotes our favoured solution. Results do not include the orbital period, P and transit epoch τ , which are treated as Gaussian priors via $P = 2.47061896 \pm 0.00000022$ days and $\tau = 2454950.822014 \pm 0.000027$ BJD_{TDB}. Quoted values are medians of marginalised posteriors with errors given by 1σ quantiles. * = parameter was fixed. We do not show the $a_{0,j}$ fitted terms, which are simply renormalisation constants and are available upon request.

Model \mathcal{M} , Data \mathcal{D}	a_{1c} [ppm] (reflec./emiss.)	a_{1s} [ppm] (beaming)	a_{2c} [ppm] (ellipsoidal)	a_{2s} [ppm] (dummy)	χ^2
$\mathcal{M}_1, \mathcal{D}_1$	0*	0*	0*	0*	162603.5431
$\mathcal{M}_2, \mathcal{D}_1$	$-7.2^{+1.8}_{-1.8}$	$0.78^{+0.85}_{-0.85}$	$-1.42^{+0.91}_{-0.92}$	$-0.27^{+0.85}_{-0.85}$	162583.4014
$\mathcal{M}_3, \mathcal{D}_1$	$-7.3^{+1.8}_{-1.9}$	$0.79^{+0.86}_{-0.86}$	$-0.77^{+0.92}_{-0.91}$	$-0.26^{+0.86}_{-0.86}$	162583.3162
$\mathcal{M}_1, \mathcal{D}_2$	0*	0*	0*	0*	161875.4005
$\mathcal{M}_2, \mathcal{D}_2$	$-6.4^{+1.8}_{-1.8}$	$0.34^{+0.86}_{-0.87}$	$-1.52^{+0.93}_{-0.94}$	$0.19^{+0.87}_{-0.87}$	161859.6732
$\mathcal{M}_3, \mathcal{D}_2$	$-6.4^{+1.8}_{-1.9}$	$0.34^{+0.86}_{-0.86}$	$-0.95^{+0.92}_{-0.92}$	$0.19^{+0.86}_{-0.87}$	161859.6095
$\mathcal{M}_1, \mathcal{D}_3$	0*	0*	0*	0*	161837.6648
$\mathcal{M}_2, \mathcal{D}_3$	$-6.5^{+1.9}_{-1.9}$	$0.22^{+0.88}_{-0.87}$	$-1.50^{+0.92}_{-0.93}$	$0.31^{+0.88}_{-0.87}$	161821.7228
$\mathcal{M}_3, \mathcal{D}_3$	$-6.7^{+1.8}_{-1.8}$	$0.23^{+0.89}_{-0.88}$	$-0.90^{+0.91}_{-0.91}$	$0.32^{+0.88}_{-0.88}$	161821.7232
Theory Expectation	$-20 \rightarrow 0$	~ 2.4	~ -2.3	0	-

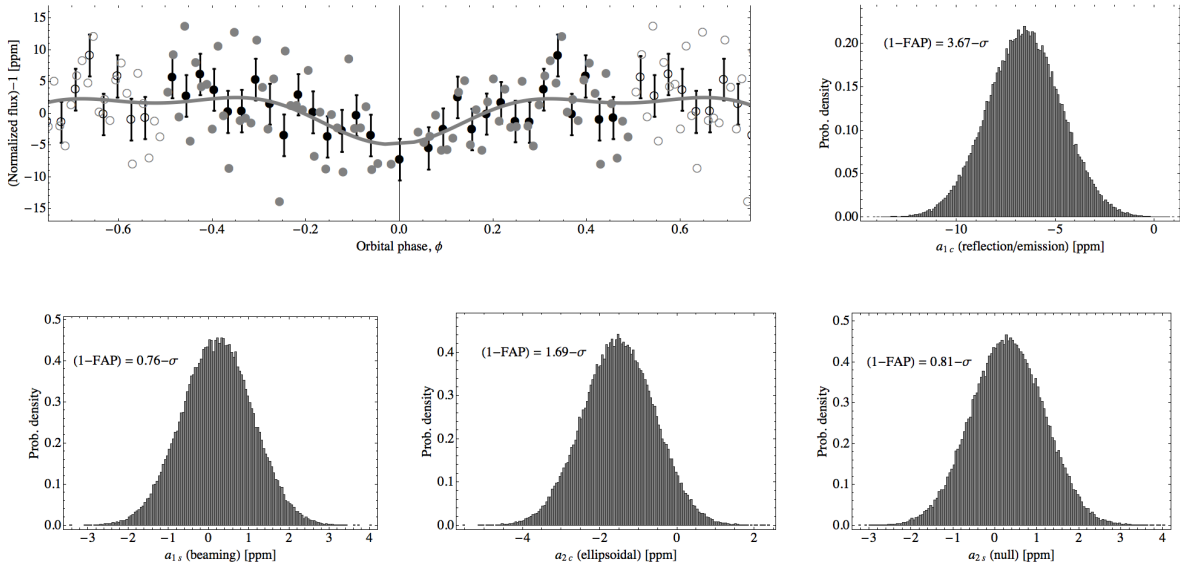


Figure 2. *Top Left:* Final fit to the phased photometry. Points without errors are the 2000-point phase binned data. Points with errors are 5000-point phase binned data. Best-fit model \mathcal{M}_2 with data mode \mathcal{D}_3 shown in solid. Note that all fits were performed on the unbinned photometry. *Top Right & Lower Panels:* Marginalised posterior distributions for the same model of four fitted parameters. Unity minus the false-alarm-probability values are provided for each parameter, based upon an odds ratio test described in §3.1.

In order to interpret the visible flux, we use the planetary atmosphere modelling code **COOLTLUSTY** (Hubeny et al. 2003). For simplicity, we adopt equilibrium chemistry with nearly Solar abundance of elements, although we leave titanium oxide and vanadium oxide (TiO and VO) out of the atmosphere model. These compounds could, if present in the upper atmosphere of a hot-Jupiter, strongly affect the atmosphere structure and the visible and near infrared spectra, by making the atmosphere more opaque in the visible and by leading to a thermal inversion if the stellar irradiation exceeds $\sim 10^9$ erg cm $^{-2}$ s $^{-1}$ (Hubeny et al. 2003; Fortney et al. 2008). We leave TiO and VO out of our calculations, however, because of the difficulty of maintaining heavy, conden-

sible species high in the atmospheres (Spiegel et al. 2009). Instead, we use an ad hoc extra opacity source κ' , as described in Spiegel & Burrows (2010).

We calculate a grid of models with κ' ranging (in cm 2 g $^{-1}$) from 0 to 0.6 in steps of 0.1 and with redistribution P_n ranging from 0 to 0.5 in steps of 0.1 (P_n represents the fraction of incident irradiation that is transported to the nightside, which is assumed in our models to occur in a pressure range from 10 to 100 mbars). For each of these 42 parameter combinations, we calculate a day-side model, a night-side model, and a model that has the same temperature/pressure structure as the dayside but that has the star

turned off, so as to calculate the emitted (and not scattered) flux (thus also giving the scattered component).

We draw several inferences from our models and the data. First, the nightside contributes negligible flux in the *Kepler*-band (always <12% of the dayside, and for most models significantly less than that), meaning that the 6.5 ppm number represents essentially the entire day-side flux.

Second, by also including the available infrared secondary eclipse data on TrES-2b (O'Donovan et al. 2010; Croll et al. 2010), we find that in our model set there must be some redistribution (but not too much) and there must be some extra absorber (but not too much). For each model, we compute a χ^2 value, including 6 data points: *Kepler*-band, *Ks*-band, and the four *Spitzer* IRAC channels (3.6, 4.5, 5.8 & 8.0 μm). Fig 3 portrays the χ^2 values of our grid of models, with the colour ranges corresponding to the χ^2 values bounding 68.3% of the integrated probability (1σ), 95.5% (2σ), 99.7% (3σ) and 99.99% (4σ). The models that best explain the available data correspond to $\kappa' \sim 0.3 - 0.4 \text{ cm}^2 \text{ g}^{-1}$ and $P_n \sim 0.3$ ($\sim 30\%$ of incident flux redistributed to the night). In particular, models with no extra absorber are completely inconsistent with observations, even on the basis of the *Kepler* data alone. The upshot is that some extra opacity source appears to be required to explain the emergent radiation from this extremely dark world. Owing to this optical opacity, our models that are consistent with the data have thermal inversions in their upper atmosphere, as in Spiegel & Burrows (2010). We note that Madhusudhan & Seager (2010) find that the IR data of TrES-2b may be explained by models both with and without thermal inversions; nevertheless, we believe that optical opacity sufficient to explain the *Kepler* data is likely to heat the upper atmosphere, as per Hubeny et al. (2003).

Finally, by computing the scattered contribution to the total flux, we find that for all parameter combinations the scattered light contributes $\lesssim 10\%$ of the *Kepler*-band flux, and for the best-fit models the scattered light is $\lesssim 1.5\%$ of the total. TrES-2b, therefore, appears to have an extremely low geometric albedo (for all models, the geometric albedo is < 1%, and for the best-fit models it is $\sim 0.04\%$). Exact values for the amount of extra optical opacity, redistribution and the albedo cannot be presently provided because inferences about them depend on unknown quantities such as the wavelength dependence of the extra opacity source and the altitude dependence of winds.

ACKNOWLEDGMENTS

We thank the *Kepler* Science Team, especially the DAWG, for making the data used here available. Thanks to A. Burrows, M. Nikku & the anonymous referee for helpful comments and I. Hubeny & A. Burrows for the development and continued maintenance of COOLTLUSTY and associated opacity database. DMK is supported by Smithsonian Instit. Restricted Endowment Funds.

REFERENCES

Baglin, A. et al. 2009, Transiting Planets, Proc. IAU Symp., 253, 71
 Basri, G., Borucki, W. J. & Koch, D. 2005, New Astronomy Rev., 49, 478

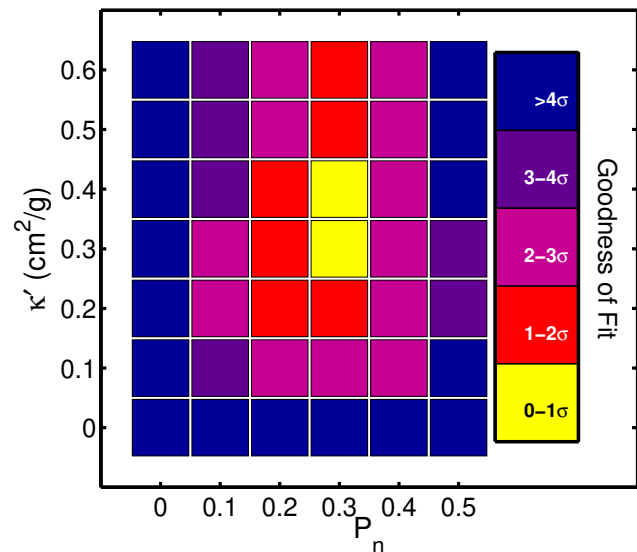


Figure 3. Goodness-of-fit for a grid of atmosphere models. The models that are consistent with available *Kepler*-band, *Ks*-band, and *Spitzer* IRAC data have moderate redistribution to the night side (P_n) and moderate extra optical opacity (κ'). Models with $\kappa' = 0$ can be ruled out on the basis of the *Kepler* data alone.

Burrows, A., Ibgui, L., & Hubeny, I. 2008, ApJ, 682, 1277
 Demory, B.-O. et al. 2011, ApJL, accepted
 Collier Cameron, A., Horne, K., Penny, A. & Leigh, C. 2002, MNRAS, 330, 187
 Croll, B., Albert, L., Lafreniere, D., Jayawardhana, R., & Fortney, J. J. 2010, ApJ, 717, 1084
 For, B.-Q., et al. 2010, ApJ, 708, 253
 Fortney, J. J., Lodders, K., Marley, M. S., & Freedman, R. S. 2008, ApJ, 678, 1419
 Hubeny, I., Burrows, A., & Sudarsky, D. 2003, ApJ, 594, 1011
 Kipping, D. M. et al. 2010, ApJ, 725, 2017
 Kipping, D. M. & Bakos, G. A. 2011, ApJ, 733, 36 (KB11)
 Leigh, C., Collier Cameron, A., Horne, K., Penny, A. & James, D. 2003, MNRAS, 344, 1271
 Madhusudhan, N., & Seager, S. 2010, ApJ, 725, 261
 Maxted, P. F. L., Marsh, T. R. & North, R. C. 2000, MNRAS, 317, L41
 Mazeh, T. & Faigler, S. 2010, A&A, 521, 59
 O'Donovan, F. T. et al. 2006, ApJ, 651, L61
 O'Donovan, F. T., Charbonneau, D., Harrington, J., Madhusudhan, N., Seager, S., Deming, D. & Knutson, H. A. 2010, ApJ, 710, 1551
 Rowe, J. F. et al. 2008, ApJ, 689, 1345
 Sirko, E. & Paczynski, B. 2003, ApJ, 592, 1217
 Snellen, I. A. G., de Mooij, E. J. W. & Albrecht, S. 2009, Nature, 459, 543
 Spiegel, D. S., Silverio, K. & Burrows, A. 2009, ApJ, 699, 1487
 Spiegel, D. S. & Burrows, A. 2010, ApJ, 722, 871
 Sudarsky, D., Burrows, A., & Pinto, P. 2000, ApJ, 538, 885
 Welsh, W. F., Orosz, J. A., Seager, S., Fortney, J. J., Jenkins, J., Rowe, J. F., Koch, D. & Borucki, W. J. 2010, ApJ, 713, 145
 Wilson, R. E. 1994, PASP, 106, 921